

doi: 10.1093/intbio/zyab008

Advance Access publication May 15, 2021 Original Article

ORIGINAL ARTICLE

Hyperglycemia minimally alters primary self-renewing human colonic epithelial cells while $TNF\alpha$ -promotes severe intestinal epithelial dysfunction

Johanna S. Dutton¹, Samuel S. Hinman², Raehyun Kim², Peter J. Attayek¹, Mallory Maurer¹, Christopher S. Sims², and Nancy L. Allbritton^{2,*}

¹Joint Department of Biomedical Engineering, University of North Carolina, Chapel Hill, and North Carolina State University, Raleigh, NC, USA, and ²Department of Bioengineering, University of Washington, Seattle, WA, USA

*Corresponding author, E-mail: nlallbr@uw.edu

Abstract

Hyperglycemia is thought to increase production of inflammatory cytokines and permeability of the large intestine. Resulting intestinal inflammation is then often characterized by excess secretion of tumor necrosis factor alpha (TNF α). Thus, hyperglycemia in hospitalized patients suffering from severe trauma or disease is frequently accompanied by TNF α secretion, and the combined impact of these insults on the intestinal epithelium is poorly understood. This study utilized a simple yet elegant model of the intestinal epithelium, comprised of primary human intestinal stem cells and their differentiated progeny, to investigate the impact of hyperglycemia and inflammatory factors on the colonic epithelium. When compared to epithelium cultured under conditions of physiologic glucose, cells under hyperglycemic conditions displayed decreased mucin-2 (MUC2), as well as diminished alkaline phosphatase (ALP) activity. Conditions of 60 mM glucose potentiated secretion of the cytokine IL-8 suggesting that cytokine secretion during hyperglycemia may be a source of tissue inflammation. TNF α measurably increased secretion of IL-8 and IL-1 β , which was enhanced at 60 mM glucose. Surprisingly, intestinal permeability and paracellular transport were not altered by even extreme levels of hyperglycemia. The presence of $TNF\alpha$ increased MUC2 presence, decreased ALP activity, and negatively impacted monolayer barrier function. When $TNF\alpha$ hyperglycemia and \leq 30 mM glucose and were combined, MUC2 and ALP activity remained similar to that of TNF α alone, although synergistic effects were seen at 60 mM glucose. An automated image analysis pipeline was developed to assay changes in properties of the zonula occludens-1 (ZO-1)-demarcated cell boundaries. While hyperglycemia alone had little impact on cell shape and size, cell morphologic properties were extraordinarily sensitive to soluble TNF α . These results suggest that $TNF\alpha$ acted as the dominant modulator of the epithelium relative to glucose, and that control of inflammation rather than glucose may be key to maintaining intestinal homeostasis.

Key words: hyperglycemia; glucose; TNF α ; colon; large intestine; intestinal epithelium; primary tissue

INSIGHT BOX

Stress hyperglycemia is often observed in critically ill patients, with intestinal epithelial cells exhibiting increased cytokine production and increased intestinal permeability. Here, the primary human colonic epithelium demonstrated a striking resistance to hyperglycemia with respect to barrier integrity and function. In contrast, tumor necrosis factor alpha ($TNF\alpha$) even at low concentrations significantly degraded barrier function and altered cell behavior with mild synergy from elevated glucose. Under these conditions, the primary human intestinal colonic epithelium was tolerant to $hyperglycemia, but intolerant to inflammatory signals such as TNF \alpha. These results suggest that control of inflammation$ rather than glucose may be key to maintaining intestinal homeostasis.

INTRODUCTION

Critically ill patients frequently develop stress-induced hyperglycemia, which portends an increased risk of morbidity and mortality [1-8]. Of patients admitted to hospitals, up to 40% experience stress hyperglycemia as defined by blood glucose levels in a non-diabetic patient greater than 7.8 mM (normal being 3.6-5.8 mM) [3, 9, 10]. This percentage increases to 80% when considering only patients in intensive care units [11]. One of the adverse outcomes for patients with stress hyperglycemia is severe infection. It is believed that the intestine, particularly the colon, which houses trillions of bacteria and other microbiota, is an important site of ingress for pathogenic organisms in these patients [12]. Supporting this hypothesis are recent clinical studies showing a relationship between sepsis and pathogenic gut bacteria, although in the absence of direct assessment of the intestinal epithelium. For example, ~30% of septic bone-marrow transplant patients were shown to be infected with bacteria found in their own colons, suggesting that the gut may be a significant source of infection [13]. Similar findings have been observed in septic patients after stem cell transplant and with congestive heart failure [14, 15].

Leakage of colonic contents into the bloodstream leading to infection is thought to occur due to altered intestinal permeability [16]. The strong barrier of the epithelial monolayer lining the colonic lumen is due in part to a high-density of tight junctions (TJ) between adjacent cells. TJ are composed of transmembrane and peripheral membrane proteins including occludin, claudins, tricellulin, and junction-associated protein (JAM). Together these proteins act to block access of luminal contents to the paracellular space [17]. The integrity and concentration of TJs found in the intestine are known to be modulated (either increased or decreased) by inflammatory factors and cytokines, including tumor necrosis factor alpha (TNF α), IL-6, IL-18, IFN- γ , and IL-1 β [18–22]. TNF α in particular has been widely reported to diminish the barrier function of the intestinal epithelium [23–27].

Nevertheless, intestinal homeostasis is dependent on continuous intercellular cross-talk, in which TNF α is an active participant. TNF α can play dual roles in both healing and damaging the intestinal epithelium and its overlying mucus layer, which is an additional barrier to microbiota [24, 28]. When intestinal cells undergo apoptosis and are shed from the epithelium, low levels of TNF α are thought to promote re-distribution of TJ proteins to maintain an impervious monolayer [29]. In contrast, high levels of $TNF\alpha$ are posited to cause epithelial micro-erosions that cannot be repaired by TJ redistribution [30]. Additionally, $TNF\alpha$ regulates epithelial cell proliferation and differentiation, with greater concentrations thought to enhance cell allocation into the secretory lineage [24]. $\text{TNF}\alpha$ influences the mucus producing goblet cell phenotype in particular, and has been shown to increase cell number, mucus secretion, and modify mucus

composition [24, 31, 32]. Alterations in the protective mucus layer and epithelial barrier integrity may allow bacterial translocation as well as increase the level of inflammatory cytokines that serve to propagate inflammation and further increase permeability

Inflammation as a result of co-existing stresses, such as that in hospitalized patients, is often increased by stress hyperglycemia and the accompanying elevated levels of inflammatory cytokines [33, 34]. However, little understanding exists of the impact of hyperglycemia and inflammatory factors, specifically TNF α , on primary human colonic permeability and cellular behavior in isolation and without other cell types/tissues [35-38]. Increases in $TNF\alpha$ have been observed in critically ill patients and those with chronic or acute hyperglycemia [1, 36, 38-40]. Efforts to identify differences in epithelial function in hospitalized patients by comparing colonic biopsy samples from healthy and critically ill patients have shown contradictory results [41, 42]. In vivo animal models have shown greater reproducibility than human studies, as have tissue-culture tumor cell lines, albeit animal and tumor cells lack normal human physiology [25, 27, 43–49]. For these reasons, improved experimental approaches are needed to study the singular and combined effects of hyperglycemia and cytokines on gut permeability in hopes of establishing proactive strategies to maintain gut integrity in the critically ill patient. In the following work, the effects of hyperglycemia and $TNF\alpha$ in isolation and together are investigated using an in vitro model comprised of stem-cell derived primary human colonic cells. This monolayer culture system incorporates a collagen hydrogel scaffold that facilitates the formation of a physiologic intestinal epithelium in a planar monolayer format [50] enabling increased sampling and assay efficiencies, as well as high-content imaging screens to be conducted. The integration of this platform with metabolism and inflammation assays, as demonstrated here, provides a valuable tool for mechanistic and predictive investigations.

MATERIALS AND METHODS

Hydrogel scaffold preparation for human cell studies

Studies utilizing primary human colonic epithelial cells were completed using a gradient cross-linked hydrogel scaffold described previously [50]. Scaffolds were prepared in cell culture inserts (Corning® Transwell® PN: 353180, Corning Inc., Corning, NY) with a polyethylene terephthalate (PET) membrane and a pore size of 0.4 μ m. Briefly, the inserts were placed within wells of a 12-well plate. Cold neutralized rat tail collagen (Supplementary Material) was added to each insert (200 µL/insert) at a thickness of 2.2 mm. Each plate was incubated at 37°C for 60 min for gelation, and then wetted with 0.5 mL of sterile phosphate

buffered saline (PBS). The wells below each cell culture insert were filled with 1.5 mL of a mixture containing 353 mM 1-ethyl-3-(3-dimethylaminopropyl) carbodiimide hydrochloride (EDC), 88 mM N-hydroxysuccinimide (NHS) and 100 mM, pH 5 2-(nmorpholino) ethanesulfonic acid (MES). During 1 h of incubation at 25°C, a gradient of crosslinking within the collagen scaffold forms [50]. The inserts with cross-linked scaffolds were removed and stored in large volumes (~1 L) of sterile water for a minimum of 24 h and up to 1 week to remove residual cross-linking reagents. The scaffolds were sterilized by incubating in 70% ethanol for 5 min, then rinsed and stored in sterile PBS at 25°C. Immediately before use, each collagen scaffold was rinsed again with sterile PBS and stored in cell culture media, which was replaced when plating passaged cells.

Human cell culture media and cell passaging

Cadaveric human intestinal epithelial tissue from the transverse colon (male, 23 y) was obtained from Carolina Donor Services (Durham, NC). The cells were expanded (RRID:CVCL_ZR41) following a previously reported monolayer culture protocol over planar collagen hydrogels (full details in Supplementary Material) [51, 52]. This hydrogel culture method allows for the rapid scale-up of intestinal epithelial cells from primary tissue compared to the widely used organoid culture technique and retains a stable karyotype for up to 20 passages [51-53]. To minimize the possibility of chromosomal aberrations, all cultures were discarded at passage 15 [52]. The primary human cells were cultured with three different media preparations; a modified expansion medium described previously (EMs) [54], cross-linked collagen scaffold expansion medium (EMT) and differentiation medium (DM). Both EMS and EMT contained Advanced Dulbecco Modified Eagle Medium/F12 (ThermoFisher, Waltham, MA) supplemented in a 1:1 ratio with Wnt, noggin, and R-spondin conditioned medium prepared from L-WRN cells (CRL-3276, ATCC, Manassas, VA, RRID:CVCL_DA06) per a previously published protocol [55]. Additional components in EMS and EM_T were: 50 ng/mL epidermal growth factor (EGF) (Peprotech, Rocky Hill, NJ), 10 mM 4-(2-hydroxyethyl)-1-piperazine ethanesulfonic acid (HEPES) (ThermoFisher, Waltham, MA), 1 mM N-acetyl cysteine (NAC) (MP Biomedicals, Santa Ana, CA), B27 supplement (ThermoFisher, Waltham, MA), 0.01 mM gastrin (Anaspec, Fremont, CA), 3 µM SB202190 (Selleckchem, Houston, TX) and 0.05 mg/mL primocin (InvivoGen, San Diego, CA). EMS additionally contained 500 nM A83-01 (Sigma-Aldrich, St. Louis, MO), and 0.5X GlutaMAX (ThermoFisher, Waltham, MA), while EM_T additionally contained 10 mM nicotinamide (Sigma-Aldrich, St. Louis, MO) and 10 nM prostaglandin 2 (PGE2) (Cayman Chemicals, Ann Arbor, MI).

The base for the formulation of DM was glucose-free DMEM (ThermoFisher, Waltham, MA). Additional components included: 10% heat inactivated fetal bovine serum (FBS, Atlanta Biologicals), 10 mM 4-(2-hydroxyethyl)-1- piperazine-ethane sulfonic acid (HEPES) (ThermoFisher, Waltham, MA), 1 mM Nacetyl cysteine (NAC) (MP Biomedicals, Santa Ana, CA), 50 ng/mL EGF (Peprotech, Rocky Hill, NJ), 500 nM A83-01 (Sigma-Aldrich, St. Louis, MO), and 0.05 mg/mL primocin (InvivoGen, San Diego, CA).

Cell passaging was performed every 5 days. First, the collagen scaffolds were removed from the 6-well plates and digested for 10 min at 37°C with 150 µL of type IV 500 U/mL collagenase (Worthington Biochemical, Lakewood Township, NJ) and 1 mL of EMs per scaffold. This mixture was centrifuged for 1 min at 600 \times g to remove the digested collagen and retain the monolayers. The monolayers were rinsed with 11 mL PBS, centrifuged again, and subsequently disassociated by incubation for 5 min at 37°C with 0.5 mM EDTA and 10 µM Y27632 (Sigma-Aldrich, St. Louis, MO) followed by vigorous micro-pipetting. After centrifugation, cells were re-suspended in EMS or EMT for expansion or cross-linked collagen scaffold studies, respectively. During subculture, one well from a 6-well maintenance/expansion plate was sub-cultured into six 12-well cell culture inserts. Cells were maintained in an incubator at 37°C and 5% CO2. Cell culture inserts with a cross-linked collagen scaffold were filled with 0.5 mL and 1.5 mL of EM_T on the apical and basal sides (upper and lower chambers), respectively. Cells were cultured on cross-linked collagen scaffolds in EMT for 5 days, with media changes occurring on days 2 and 4. On day 5, the medium was changed to DM for 2 days, and studies with high glucose DM typically began on day 7. Media was changed daily from days 5 to 8, with fixation or analysis on

Hyperglycemia and TNF α studies

The stock TNF α solution (Peprotech PN: 300-01A, Rocky Hill, NJ) was prepared at a concentration of 10 µg/mL in 3% bovine serum albumin (BSA) (ThermoFisher, Waltham, MA). Studies were completed at concentrations of 20, 40, and 60 ng/mL. The stock glucose (Sigma-Aldrich, St. Louis, MO) was prepared at a concentration of 500 mM in PBS and filter sterilized. Concentrations of 5, 15, 30, and 60 mM glucose were used.

Measurement of transepithelial electrical resistance

Transepithelial electrical resistance (TEER) was used to assess the barrier integrity of confluent monolayers using an EVOM2 epithelial Volt/Ohm meter (World Precision Instruments, Sarasota, FL). The instrument uses a STX2 chopstick electrode in contact with the apical and basal chambers to determine the resistance across the monolayer. The output of this assay is normalized to Ω cm² by multiplying the measured resistance value by the surface area of the well (0.9 cm²) and reported as a relative percent change in TEER over the experimental time frame (i.e. relative TEER). Relative TEER was determined by subtracting the TEER value obtained on culture day 5 from the TEER value obtained on culture day 9 and calculating the percent change, thus minimizing inter-well variability [56, 57]. The average of three separate wells was recorded for each condition tested.

Measurement of monolayer permeability

A second measure of barrier integrity was permeability of the monolayer to Lucifer yellow CH dipotassium salt (LY) (Sigma-Aldrich, St. Louis, MO). LY was prepared in Hank's Balanced Salt Solution (HBSS with Ca²⁺ and Mg²⁺, ThermoFisher, Waltham, MA) at a concentration of 2 mM. For each well of a 12 wellplate (surface area of 0.9 cm²), 0.5 mL of LY was added to the apical chamber at a concentration of 200 µM in HBSS. The basal chamber was filled with 1.5 mL of HBSS with no LY. Samples were stored at 37°C and 5% CO₂ for 4 h, after which the solution in the basal chamber was gently mixed and sampled. Permeability was determined by measuring the LY fluorescence (ex: 430 nm, em: 535 nm) in a Spectramax M5 plate reader (Molecular Devices

Corporation, San Jose, CA). The apparent permeability was calculated using the following equation:

$$Permeation = \frac{[C_B] \times V}{A \times t \times [C_A]}$$

where $Permeation = P_{app}$ (apparent permeability of LY (cm/s); [C_B] = LY concentration in the basal sample calculated using a standard curve (μ M); V = volume in the basal reservoir (1.5 cm³); A = membrane surface area (0.9 cm²); t = incubation time(4 h = 14400 s); $[C_A] = LY$ concentration in the apical chamber $(200 \mu M).$

Identification of enterocytes from the presence of alkaline phosphatase

Enterocytes were identified in cell monolayers by the presence of alkaline phosphatase (ALP) activity. During culture, the live cells were incubated at 37°C for 30 min with ALP substrate from the Vector Red Alkaline Phosphatase Substrate Kit (Vector Laboratories PN: SK-5100, Burlingame, CA). The ALP substrate was prepared in pH 8.4, 150 mM Trizma buffer. Cells were fixed with 4% paraformaldehyde (1 mL in the apical chamber and 1 mL in the basal chamber) for 15 min and rinsed with PBS. Cellular DNA was stained with Hoechst 33342 (2 µg/mL) (Sigma-Aldrich PN: B2261, St. Louis, MO) for 1 h at 25°C. Finally, cells were rinsed in PBS, and stored in 0.1% NaN3 at 4°C until imaging. The quantification of alkaline phosphatase per condition was determined by dividing the ALP stained area by the DNA stained area for each of three separate wells. The area for each well was 3.8 cm² and contained approximately 10⁶ cells [50, 52].

Identification of goblet cells by intracellular MUC2

After culture, cell monolayers were fixed as above. Cells were then rinsed with PBS (the basal chamber of the scaffold system was not used following this rinse step) and permeabilized by incubation in 0.5% Triton X-100 for 20 min at 25°C. The apical chamber was then rinsed with immunofluorescence (IF) wash (PBS, 0.2 vol % Triton X-100, 0.05 vol % Tween-20, 1 mg/mL BSA, 0.5 mg/mL sodium azide) once, and blocked with 10% donkey serum (Jackson Immunoresearch PN: 017-000-121; West Grove, PA) in IF wash for ≥ 1 h at 25°C. After aspiration, primary MUC2 antibody (Invitrogen PN: MA5-12345, Carlsbad, CA) was diluted 1:1000 in IF wash and added to the cells, which were stored overnight at 4°C. After aspiration of the primary antibody solution, the wells were rinsed three times (for \geq 5 min each) before application of the secondary antibody, AlexaFluor 488 (Jackson Immunoresearch PN: 711-545-152, West Grove, PA) prepared in IF. Simultaneous with the secondary antibody incubation, cellular DNA was stained with Hoechst 33342 (2 µg/mL) (Sigma-Aldrich PN: B2261, St. Louis, MO) for 1 h at 25°C. After a final rinse in PBS, samples were stored in 0.1% NaN3 at 4°C until imaging. The goblet cell quantification per condition was determined by dividing the MUC2 stained area by the DNA stained area for each of 3 separate wells. The area for each well was 3.8 cm² and contained $\sim 10^6$ cells [50, 52].

Quantification of ALP enzyme activity

Total protein was determined using the Pierce Protein Assay (ThermoFisher PN: 23225, Waltham, MA). Samples were prepared by digesting the collagen scaffold with 150 µL collagenase per well, vigorous pipetting, and storage at 37°C for 10 min. These samples were centrifuged and rinsed with 3 mL PBS. After centrifugation and aspiration, each sample was re-suspended in 200 µL cold RIPA lysis buffer (ThermoFisher, Waltham, MA) with inhibitor cOmplete™, Mini Protease Inhibitor Tablets (Roche, Branchburg, NJ) per manufacturer's instructions, then transferred to microcentrifuge tubes. Each tube was stored at 4°C for 20 min and vortexed every 5 min. Finally, samples were centrifuged at 4° C for 10 min at 2200 \times g. The collected supernatant was stored at -20° C until use in the total protein assay or ALP activity measurements.

The Sensolyte Luminescent ALP substrate (Anaspec PN: 72122, Fremont, CA) was used as specified by the manufacturer to quantify the ALP activity (cell lysate) in units of picograms, normalized by total protein per sample. Each value was an average of three independent sample preparations per condition.

Measurement of IL-8 and IL-1 β

The concentration of IL-8 was determined using the Human IL-8 Uncoated ELISA Kit (Invitrogen PN: 88-8086-88, Carlsbad, CA) per the user manual. Supernatant samples were diluted 1:20, and three separate wells were measured per condition. IL-1 β was measured using the Human IL-1 β Uncoated ELISA Kit (Invitrogen PN: 88-7261-88, Carlsbad, CA) following the user manual. Supernatant samples were diluted 1:2, and three separate wells were measured per condition.

Cell immunoassay for zonula occludens-1

Cell monolayers were fluorescently stained for the tight junction protein (zonula occludens-1 – ZO-1) to identify cell boundaries by confocal microscopy (see below). After culture, the cell monolayers were rinsed with PBS and fixed with 100% methanol (1 mL in each of the apical and basal chambers) at -20° C for 1 h. After fixation, the chambers were rinsed with PBS twice. The basal chamber was not used after this rinse step. The apical chamber was then rinsed once with IF wash and stored in IF wash for at least 1 h for blocking without additional animal protein block. The IF wash was composed of 8 mM sodium azide (NaN₃), 0.1% BSA, 2 μ L/mL Triton-X 100, and 0.5 μ L/mL Tween-20 in PBS. After aspirating the IF wash from each well, primary ZO-1 antibody (Proteintech PN: 21773-1-AP, Rosemont, IL) was diluted 1:1000 in IF wash and added to the apical chambers, which were stored overnight at 4°C. After aspiration of the primary antibody solution, the wells were rinsed three times for at least 5 min each before application of the secondary antibody AlexaFluor 594 (Invitrogen PN: R37119, Carlsbad, CA) prepared in IF wash (1 drop/mL). Simultaneous to the secondary antibody incubation, cellular DNA was stained with Hoechst 33342 (2 µg/mL) (Sigma-Aldrich PN: B2261, St. Louis, MO) for 1 h at 25°C. Samples were stored at 25°C for 1 h prior to a final rinse in PBS and storage in 0.1% NaN3 at 4°C until imaged.

Measurement of cell boundary properties by confocal microscopy

Images were acquired using an inverted Olympus Fluoview 3000RS (Olympus America, Waltham, MA) utilizing UPLSAPO-4× (N.A. 0.16), LUCPLFLN-20 \times (N.A. 0.45), and UPLSAPO-40 \times (N.A. 0.95) objectives in conjunction with a galvanometer scanner. The system is equipped with laser diodes at 405, 488, 561, and 640 nm and two 2-channel GaAsP PMT detectors. A maximum intensity projection of the acquired Z-stacks was performed in CellSens Dimension v1.18 to convert the Z-stacks to flattened 2D images with an XY resolution of 0.62 µm/pixel for image segmentation. Z-step size was variable (5.5–8.8 um), dependent on the sample thickness and morphology.

A custom MATLAB script was written to perform image processing and analysis (Supplementary Fig. 1). Each 2D image was median filtered with a 3×3 kernel to de-noise the image while maintaining edges (Supplementary Fig. 2a) [58]. The resultant median filtered images were background subtracted using a Top-hat filter with a disk structuring element (8-pixel radius) (Supplementary Fig. 2b). The background subtracted images were thresholded using Otsu's method (Supplementary Fig. 2c) [59]. The thresholded images were skeletonized and objects smaller than 5 pixels were removed (Supplementary Fig. 2d) [60]. The endpoints of the skeleton images were identified, and morphological closing operations were performed on the endpoints in order to connect any incomplete paths (Supplementary Fig. 2e). The skeleton images were then pruned to remove any branches that were <5 pixels.

To reduce over-segmentation, a MATLAB function was designed to remove skeleton segments that were less prominent than the surrounding segments. First, the gradient of the median filtered images was calculated. Then the branch points of the skeletons were removed from the skeleton images so that each segment was an individual object. These skeleton segment images were applied as a mask to the gradient image and the median gradient value (MGV) was calculated for each segment. Segments were removed from the skeleton image if their MGV was <0.3 the mean of the 10 closest neighboring segment MGVs. This generated the final skeleton images (Supplementary Fig. 2f).

The final skeleton images were inverted and eroded with a disk structuring element (2-pixel radius) to remove small objects and to generate seeds for a watershed algorithm (Supplementary Fig. 2g). The seeds were used to impose a minimum value on the median filtered images (Supplementary Fig. 2h) [61]. A watershed transform was executed on the resultant image and inverted (Supplementary Fig. 2i and j) [62]. The endpoints of the final skeleton images were dilated with a disk structuring element (radius = 1 pixel). Any objects in the inverted watershed images that overlapped with the dilated skeleton endpoints were removed from the inverted watershed image (Supplementary Fig. 2k). All objects were then property filtered by size (remove objects with area < 100 pixels and >2000 pixels), solidity (remove objects with solidity <0.6), and Euler number (remove objects with Euler number < 1) (Supplementary Fig. 21). Finally, the perimeter, area, solidity, circularity, eccentricity, and border fluorescence intensity were obtained for each remaining object.

The automated tight junction segmentation was compared to manually annotated segmentation. Random, 150 \times 150 pixel (8649 μm^2) regions of interest (ROIs) were selected from the 2D fluorescence tight junction images (n = 22). The tight junctions were manually annotated and compared to the results of the image analysis method. Compared to the manually annotated segmentations, the automated analysis resulted in an oversegmentation of 1.4 \pm 2.5% of cells (1.0 \pm 1.2 per ROI) and an under-segmentation of 0.5 \pm 1.1% of cells (0.4 \pm 0.8 per ROI). The automated tight junction analysis resulted in a sensitivity of 47 \pm 15% and a positive predictive value (PPV) of 99 \pm 1%. The relatively low sensitivity is due to the program rejecting any objects that it considered incorrectly or not fully segmented; however, the high PPV indicates that any object that was kept had a high likelihood of being a true cell.

Statistical analysis

GraphPad Prism 8.3.0 (GraphPad Software, San Diego, CA) was used to perform statistical analysis on all assays except for cell morphology data. For single variable analysis, one-way ANOVA with Tukey's test for multiple comparisons was used. To compare synergistic effects of glucose and $TNF\alpha$, two-way ANOVA with Tukey's test for multiple comparisons was used. Statistical significance is defined as follows: * for P \leq 0.05, ** for P < 0.01, *** for P < 0.001 and **** for P < 0.0001. All data and error bars represent mean \pm one standard deviation unless otherwise noted.

RStudio (version 1.2) was used to perform statistical analysis and effect size measurements for the cell morphology data. Circularity and perimeter measurements were directly subjected to analysis, while area estimates were log transformed to follow a normal distribution prior to hypothesis testing. The 'glm' function in RStudio (version 1.2) was used to fit linear models of these parameters for each glucose and TNF α level, providing effect size measurements (beta). Pairwise contrasts of levels within each factor (glucose or $TNF\alpha$) were performed using Tukey's test in the 'multcomp' package.

RESULTS AND DISCUSSION

Description of the model human colonic epithelium

Human primary colonic epithelial cells were cultured on a gradient cross-linked scaffold of collagen hydrogel (Fig. 1a) [50]. This culture system enables the formation of a self-renewing primary human colonic epithelial monolayer that retains mechanical stability over long culture times. The collagen surface in contact with the cells is weakly crosslinked to yield a stiffness mimicking that of in vivo colonic epithelium (400 Pa) [50]. In contrast, the base of the thick collagen hydrogel is extensively cross-linked, rigidly anchoring the scaffold to the base of a tissue insert to prevent deformation over multiple weeks of culture. Prior work has demonstrated that this culture format preserves a richer feature set (transport, metabolism, barrier integrity, and cell type) compared to that supported by plastic culture surfaces coated with a thin layer of extracellular matrix [50, 63, 64]. Since the scaffolding possesses mechanical properties and biomolecular cues similar to those measured in vivo, both stem/proliferative cells and differentiated lineages are present in the culture system [52]. An additional asset of this culture system is that the medium within the basal and luminal reservoir is readily accessible for sampling and analytical

The gradient cross-linked scaffold system with primary human colonic epithelium was used to study the impact of hyperglycemia and $TNF\alpha$ on stem/proliferative cells as well as on the most prevalent differentiated cell types. To assess the impact of microenvironmental conditions on stem/proliferative cells, the cells were cultured over the scaffolding within EM_T, a medium rich in Wnt-3a, R-spondin, and Noggin, which supports stem cells and promotes cell proliferation. Differentiated intestinal epithelial cells were formed over the scaffold by removing these growth factors (culture under differentiation medium, or DM) enabling the assessment of the impact of hyperglycemia and TNF α on both lineage allocation and terminal cell physiology, i.e. absorptive colonocyte and secretory goblet cell behaviors (Fig. 1b). Most conventional tissue culture media contains high levels of glucose (17.5 mM) that are equivalent to the untreated human diabetic state. Thus, for these experiments

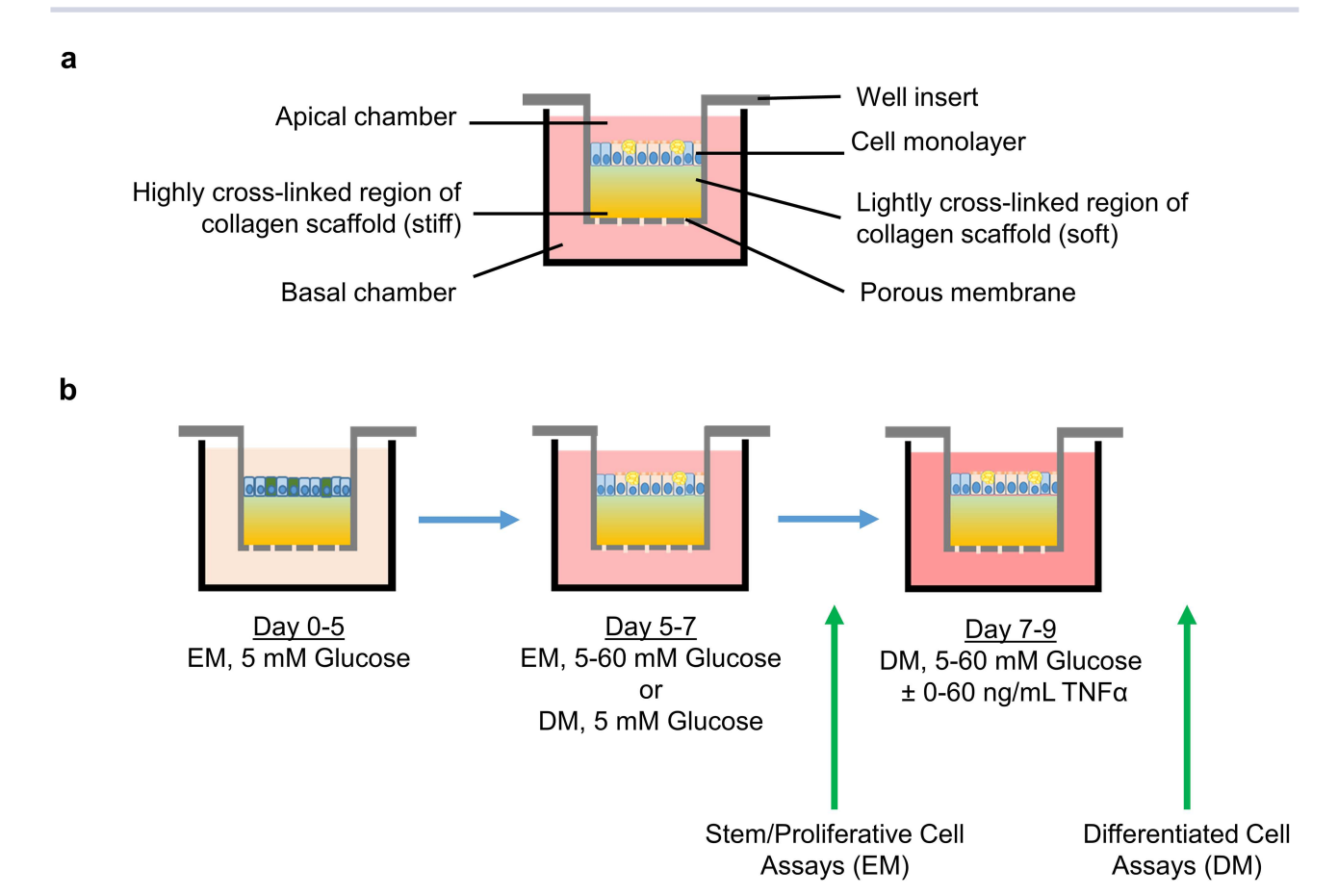


Figure 1. Diagram of model and experimental timeline. (a) The model used in this study consists of a monolayer of primary human colonic epithelial cells grown over a collagen hydrogel support within a cell culture insert. The collagen hydrogel is covalently crosslinked to strengthen the base and secure it within the insert throughout culture. Basal and luminal compartments are accessible for reagent sampling and exposure treatments. (b) The colonic epithelial cells are seeded within the chamber inserts and expanded for 5 d under EM. For representative images of these cells during expansion, see references [50, 52, 63], and. The cells are then further cultured in EM or DM for 2 days and then assayed or further differentiated and assayed. TNF α exposure treatments are thereafter conducted during the final 2 d of culture.

the cells were cultured in 5 mM glucose from their first passage and for all additional expansion and propagation. Thereafter, experimental cell culture media contained levels of glucose that simulate normoglycemia (5 mM), acute hyperglycemia (15 mM) and extreme hyperglycemia (30 and 60 mM) [9, 10]. TNF α concentrations (20, 40, and 60 ng/mL) were selected from preliminary culture screens in which measurable perturbations to barrier function (e.g. TEER and ZO-1 deformation) were induced and are consistent with the known bioactive concentrations and the measured receptor affinities for $TNF\alpha$ [65-68].

Cell differentiation in presence of hyperglycemia and $TNF\alpha$

Lineage allocation of differentiated intestinal epithelial cells drives overall function of the tissue, and has been shown to be regulated by canonical signaling pathways (e.g. Wnt, Notch), energy sources, and inflammation [69]. Glucose is the primary energy source for intestinal stem cells, but the differentiated absorptive enterocytes that line the colonic lumen preferentially metabolize short chain fatty acids [70]. Additionally, inflammatory factors such as $TNF\alpha$ generally induce Notch signaling [71], thus favoring absorptive lineages. To evaluate the effect of hyperglycemia and TNFα-induced inflammation on lineage allocation towards absorptive vs. secretory cells, cells were cultured under high glucose and/or $TNF\alpha$ and compared to those cultured under physiologic conditions (5 mM glucose and no added TNF α). Stem/proliferative cells, i.e. cells cultured in EM_T, were differentiated in the presence of high glucose followed by assay of cell-surface ALP and intracellular MUC2 (Fig. 2a, Supplementary Fig. 3). Under all conditions of elevated glucose (15, 30, 60 mM) without TNF α , cell-surface ALP and MUC2 presence were significantly reduced relative to those of the control samples suggesting that hyperglycemia decreased formation of both colonocytes and goblet cells during lineage allocation or tissue differentiation (Fig. 2b). As TNF α was increased in the presence of a normal glucose concentration, the amount of MUC2 increased relative to that of controls suggesting that TNF α alone also enhanced the formation of goblet cells (Fig. 2c). An increase in mucus production upon TNF α exposure has previously been observed in a rectal cancer cell line [31] which conflicts with the status of TNF α as a known inducer of Notch signaling [71]. Our observation from healthy colon cells may be indicative of a protective response of normal epithelium, as $TNF\alpha$ has also been implicated to alter the expression, secretion and composition of intestinal mucus as part of mitogen-activated protein kinase (MAPK)-regulated epithelial restitution and regeneration

Exposure to moderate levels of TNF α (20 ng/mL) did not modulate the impact of increased glucose levels on cell-surface

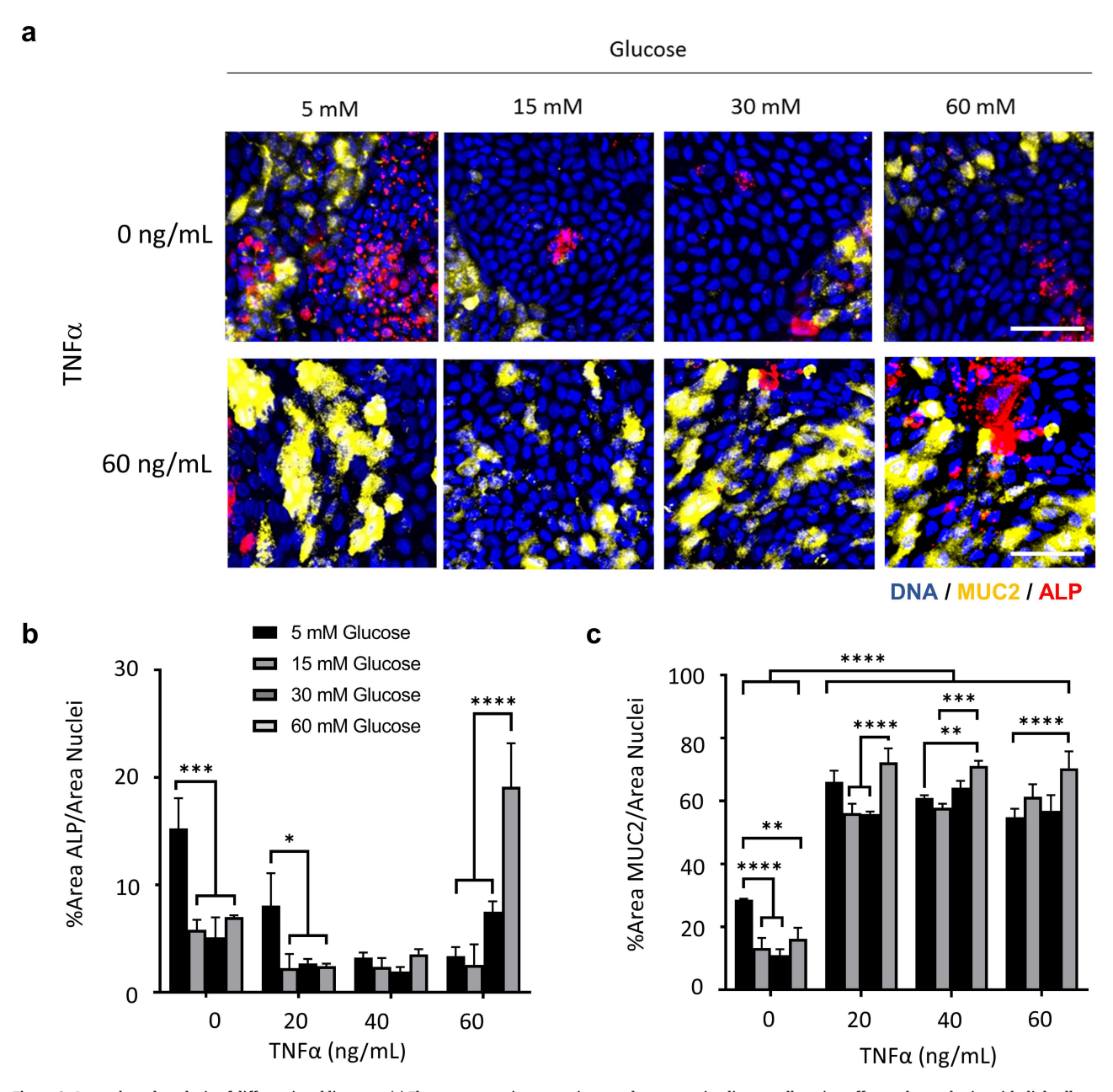


Figure 2. Image based analysis of differentiated lineages. (a) Fluorescence microscopy images demonstrating lineage allocation effects when colonic epithelial cells are exposed to elevated glucose and/or TNFα. Scale bar represents 50 um. (b) Shown on the vaxis is the ALP⁺ area divided by the Hoechst 33342⁺ fluorescence for each treatment (5–60 mM glucose, 0–60 ng/mL $TNF\alpha$, n = 3). (c) Area quantification of $MUC2^+$ area for each condition (5–60 mM glucose, 0–60 ng/mL $TNF\alpha$, n = 3).

ALP activity. However, at the highest concentrations of $TNF\alpha$ and glucose (60 ng/mL and 60 mM, respectively), significantly more cell-surface ALP was present in the cultures, suggesting that when elevated together glucose and $TNF\alpha$ may increase colonocyte numbers or ALP expression to exert a protective effect. Since ALP is located intracellularly as well as on the cell surface, total ALP activity (membrane attached and intracellular) was also measured (Fig. 3a). In the presence of hyperglycemia alone, total ALP activity did not change suggesting that while the cells maintained total ALP enzyme, the cells were sequestering ALP intracellularly rather than transporting the enzyme to the cell surface. In the presence of $\mathsf{TNF}\alpha$ and elevated glucose, total ALP activity decreased suggesting that the cells were unable to support synthesis of this important metabolic enzyme.

Cytokine production by differentiated cells in presence of hyperglycemia and $TNF\alpha$

 $TNF\alpha$ induces secretion of inflammatory cytokines, most notably interleukin 8 (IL-8) [72]. Secreted IL-8 production by differentiated cells cultured under hyperglycemic conditions was measured to determine whether elevated glucose alone induced inflammatory signaling (Fig. 3b). Even under the most severe hyperglycemic conditions, no significant difference was observed in the IL-8 production relative to that of the normoglycemic control. As TNF α was increased in the presence of either normo- or hyperglycemia, there was a significant increase in IL-8 secretion relative to that without added TNF α . High glucose concentrations (60 mM) potentiated IL-8 secretion suggesting a synergistic effect of these two stimuli on tissue

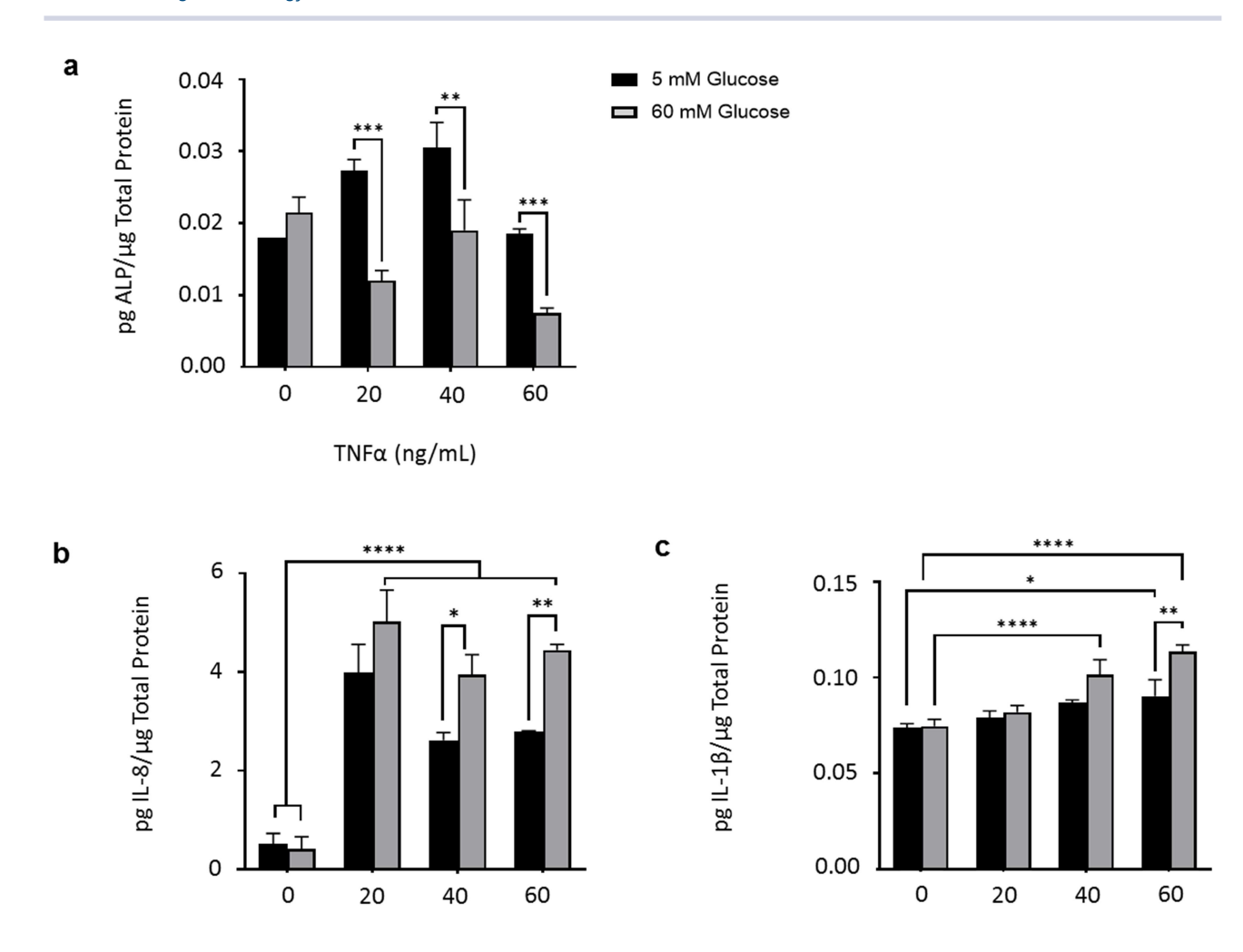


Figure 3. Measurement of ALP activity, IL-8 secretion or IL-1 β secretion. (a) Quantification of intracellular plus cell-surface alkaline phosphatase activity normalized to total cell monolayer protein content for 0-60 ng/mL TNFα in conjunction with low (5 mM) and high (60 mM) glucose (n = 3). (b) Quantification of interleukin 8 (IL-8) secretion into the luminal medium compartment normalized to total cell monolayer protein content for 0-60 ng/mL TNFa in conjunction with low (5 mM) and high (60 mM) glucose (n = 3). (c) Quantification of interleukin 1 β (IL-1 β) secretion into the luminal media compartment normalized to total cell monolayer protein content for 0–60 ng/mL TNF α in conjunction with low (5 mM) and high (60 mM) glucose (n = 3).

inflammation. In addition to IL-8, TNF α also measurably increased secretion of cytokine IL-1 β and this secretion was enhanced at high glucose concentrations (Fig. 3c). While hyperglycemia alone has been linked to an increase in cytokine secretion by immune cells, the colonic epithelial cells required the presence of TNF α for increased cytokine secretion relative to normoglycemic cells [36, 37, 73].

TNFα (ng/mL)

Monolayer integrity

For bacterial invasion from the intestinal lumen into the blood stream, the barrier integrity of the epithelial monolayer must be compromised. To determine the effect of hyperglycemia and TNF α on monolayer integrity, two common methods were used: transepithelial electrical resistance (TEER) and Lucifer yellow (LY) permeability. There was no significant difference in TEER when samples were cultured in the varying glucose concentrations (5-60 mM) suggesting that glucose alone had no impact on epithelial-cell barrier integrity under these conditions (Fig. 4a). In contrast, even low levels of TNFα (20 ng/mL) negatively impacted TEER and this decline was enhanced at mid-to-high levels of TNF α (40–60 ng/mL) (Supplementary Fig. 4). These data are similar to that obtained when immortalized Caco-2 cells are exposed to TNF α [74, 75].

 $TNF\alpha (ng/mL)$

While TEER is a measure of ion movement, LY transit through the epithelium is a more accurate measure of barrier integrity since LY is not transported across the colonic epithelium (unlike ions) [50]. At all glucose levels, the measured permeability fell below 10^{-7} cm/s indicative of an intact and confluent monolayer of human colonic epithelial cells (Fig. 4b) [50]. There was no significant increase in permeability when $TNF\alpha$ was added up to 40 ng/mL (for any glucose concentration). The highest concentration of TNF α (60 ng/mL) significantly increased monolayer permeability irrespective of the glucose concentration. Taken together with the TEER data, hyperglycemia (5-60 mM) alone or in the presence of low concentrations of $TNF\alpha$ did not alter the barrier function of this primary human colonic epithelial monolayer. However, greatly elevated TNF α (60 ng/mL) did significantly impair the monolayer's barrier function at all glucose concentrations, likely due to cellular death and delamination from the support (Fig. 5). Since inflammation can be highly localized in tissues with the presence of large numbers of infiltrating

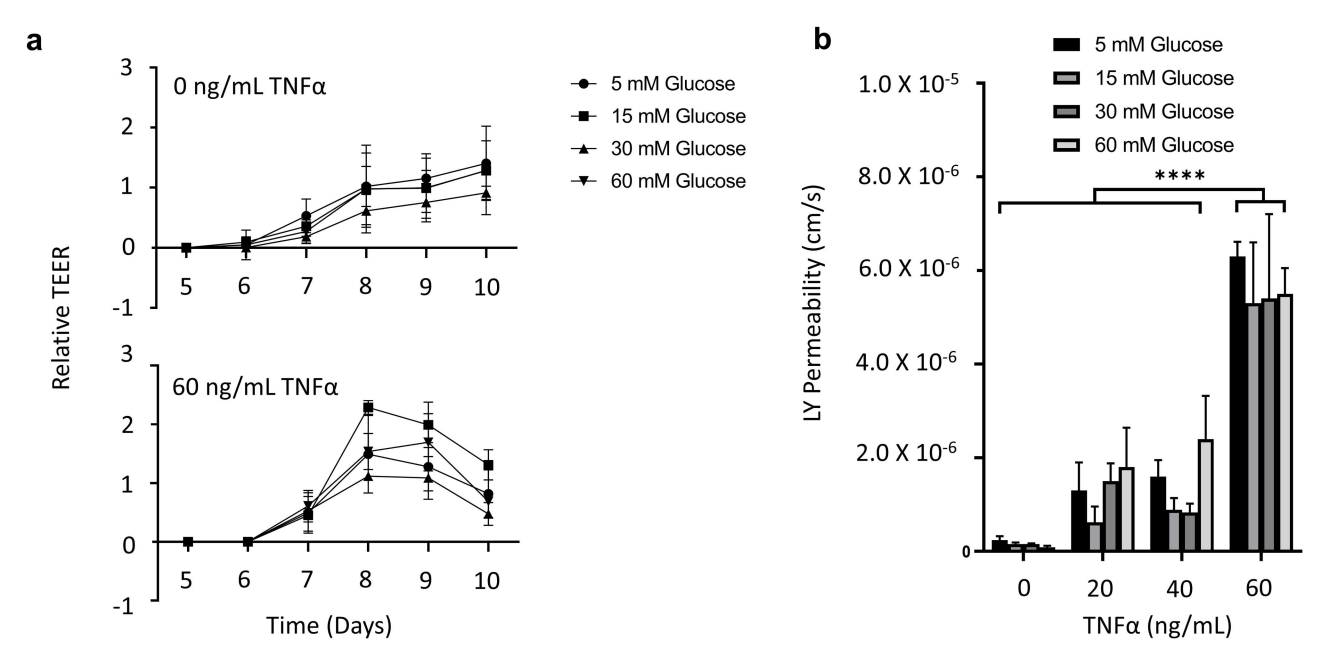


Figure 4. Measurement of monolayer barrier integrity. (a) TEER measurement versus time in the presence of 0 or 60 ng/mL TNFα and varying glucose concentrations (5-60 mM, n=3). No significant differences were observed between TEER measurements (P>0.05). Relative TEER was determined by subtracting the TEER value obtained on culture day 5 from the TEER value obtained on culture day 9 and calculating the percent change. (b) Permeability coefficient for LY under varying conditions (5-60 mM glucose, 0-60 ng/mL TNF, n = 3).

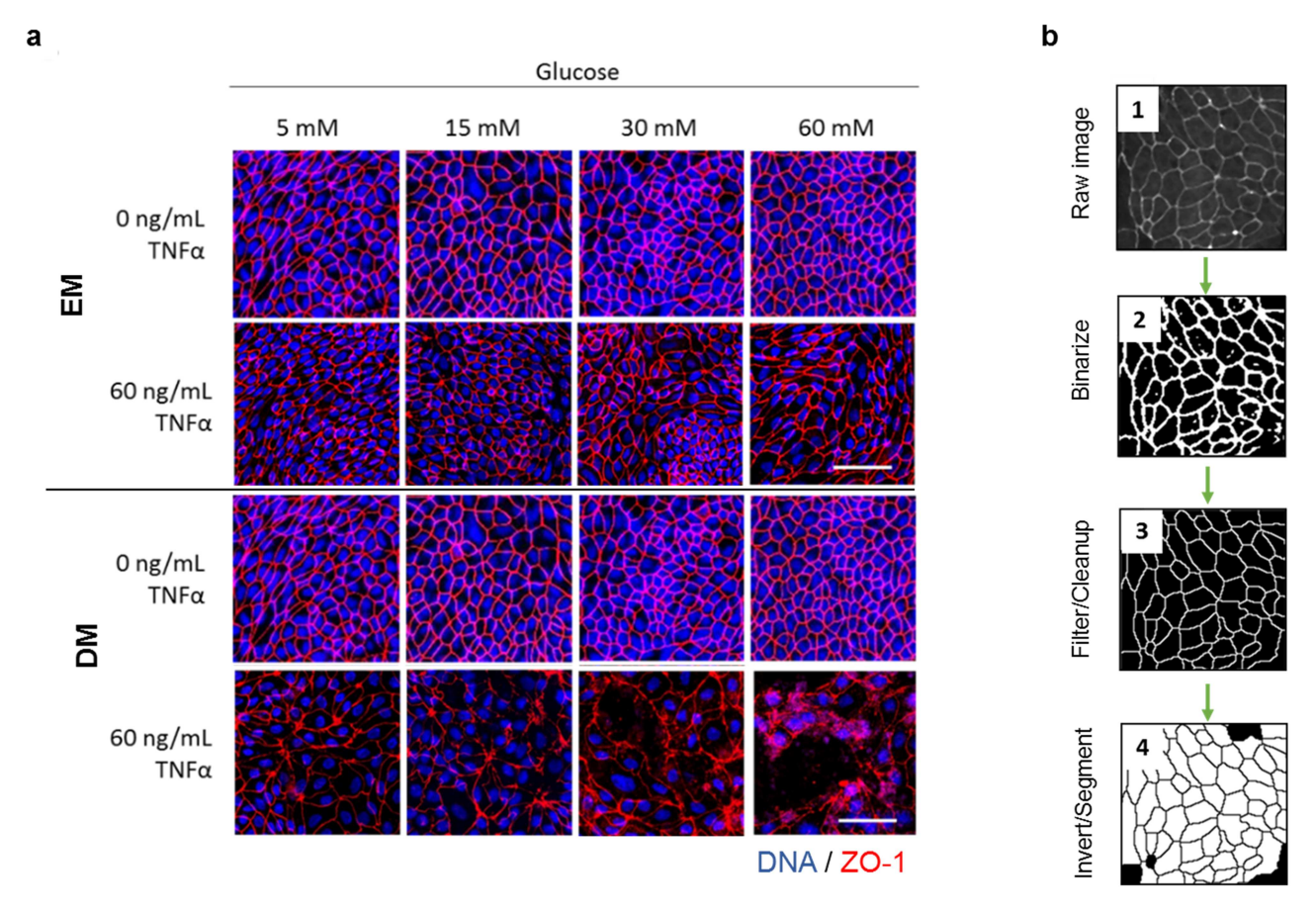


Figure 5. Imaging and perturbation analysis of ZO-1 properties. (a) Fluorescence microscopy images of ZO-1 immunofluorescence and Hoechst 33342-DNA staining in the presence of elevated glucose and/or $TNF\alpha$. The response of both stem/proliferative cells (EM) and differentiated cells (DM) was assessed. Scale bar represents 50 μm . (b) Schematic of the automated image analysis pipeline for ZO-1 boundary segmentation and morphological profiling.

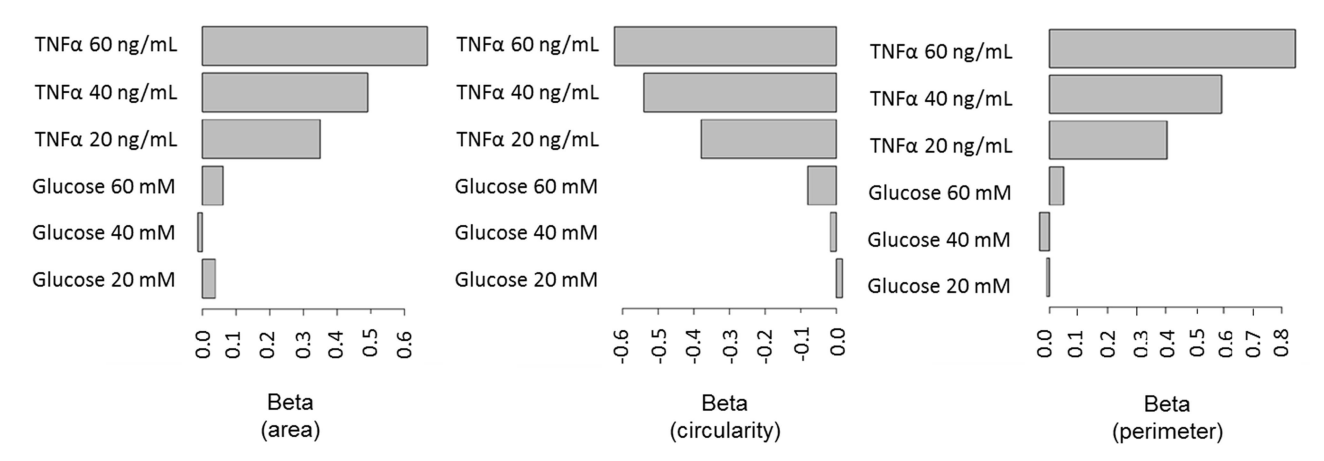


Figure 6. Area, circularity, and perimeter effect size measurements (beta) derived from linear models of TNF α exposure.

immune cells, it is conceivable that localized intestinal regions experience barrier loss with potentially organism-wide impact once the very large numbers of colonic bacteria gain access to the blood stream.

Cell morphology

To assess whether more subtle cell morphologic changes might occur than can be measured by TEER and permeability, changes to the tight junction protein, ZO-1, including its location and patterning, were assessed. Monolayers with hyperglycemia, added TNF α , or a combination of the above, were stained for ZO-1 and DNA and imaged using confocal microscopy (Fig. 5a). The tight junctions of cells cultured in DM displayed greater fragmentation upon TNF α exposure than that cultured in EM. This is in agreement with previous studies in colonic organoids, which showed that colonoids enriched in differentiated cells were more leaky than those enriched in stem/proliferative cells [47]. ZO-1 staining patterns were quantitatively assessed using a customized analysis pipeline (Fig. 5b, extended description in Supplementary Figs 2, 6, 7). Cell size as measured by ZO-1-bounded area significantly increased relative to that of the controls for both augmented glucose or added TNF α alone (Supplementary Fig. 8). The increase in cell area was not potentiated when glucose and TNF α were applied in combination (Supplementary Fig. 8). To better understand the comparative effects of these treatments, all data were fit to linear models, where effect sizes were calculated as standardized coefficients (beta, Fig. 6). Beta can be interpreted as the standard deviation increase in each morphological parameter when the concentration of $TNF\alpha$ or glucose is increased by one standard deviation, and a greater magnitude of beta is indicative of a larger effect compared to control conditions (i.e. 5 mM glucose, 0 ng/mL TNF α). For TNF α exposure, the magnitude of beta increases in a dose-dependent fashion for all measured morphological parameters (beta > 0.35), indicative of a strong correlation between TNF α levels and cellular morphology. Colonic epithelial cells exposed to $TNF\alpha$ demonstrated disrupted morphology which included a flattened and more squamous-like appearance (Fig. 5a). The decrease in circularity was also easily observed from the irregularly shaped borders of the flattened cells. In contrast, the beta value was not consistently altered (beta < 0.1) for each morphological measure under glucose exposure. Interactions of TNF α and glucose were also tested but did not provide significantly improved

fits (likelihood ratio test, P > 0.1 in all cases), indicating that hyperglycemic conditions did not significantly exacerbate the effects of TNF α exposure in regards to cell morphology changes. Comparable to permeability and TEER, the impact of $TNF\alpha$ dominates that imposed by hyperglycemia. These results are in contrast to those reported previously for Caco-2 cells cultured in the presence of elevated glucose [76]. Derived from a human epithelial colorectal adenocarcinoma, the status of the Caco-2 line as a heterogeneous tumor cell population has resulted in transport and metabolic activities that vastly differ from healthy colonic tissue [77, 78], with many studies suggesting Caco-2 cells to be more representative of small intestinal than colonic epithelium [79, 80]. The model utilized in the present study, consisting of primary healthy colonic epithelial cells cultured over a hydrogel support, may be more physiologically relevant for colonic metabolism and inflammation assays. Moreover, image analysis algorithms similar to that developed here could enable high-content assessments of inter-individual effects on cell morphology.

CONCLUSIONS

Organ-on-chip platforms that incorporate primary human cells to recapitulate human physiology are poised to revolutionize clinical science [81]. The studies described here used such a model system to emulate the physiology of the intestinal epithelium. The manipulation of experimental variables and quantitative data collection from our planar collagen hydrogel platform enable facile and well controlled metabolism and inflammation experiments that are not possible with in vivo studies using animal or human subjects [82], and are difficult to implement in 3D culture systems, particularly when performing high-content image screens. Under permissive culture conditions, primary human gastrointestinal stem cells spontaneously differentiated into the cell types that make up normal intestinal epithelium [52]. There is no need to molecularly engineer the cells or engage in extended differentiation protocols as is required with human induced pluripotent stem cells (iPSCs) [83]. Unlike tumor cell lines such as Caco-2, which have been utilized in the vast majority of in vitro intestinal metabolism and inflammation studies [24, 71], adult primary cells lack genetic mutations and other physiologic abnormalities to better represent human physiology, particularly when cultured on a physiologic scaffold possessing the proper stiffness and mechanical cues for stem cell propagation and differentiation

In the current report, the roles of hyperglycemia and select inflammatory cytokines on colonic epithelium were investigated. The work strove to improve the experimental parameters of in vitro platforms through the use of normal, primary colonic epithelium with comparisons made to control tissue cultured under physiologic glucose concentrations, rather than the high glucose concentrations used in standard tissue culture. When compared to these normal conditions, the colonic tissue under hyperglycemic conditions displayed decreased MUC2 presence and diminished ALP activity. Although it has been suggested that hyperglycemia may alter intestinal permeability and paracellular transport, these factors were not affected even at extreme levels of hyperglycemia in our model system. In the absence of hyperglycemia, exposure to $TNF\alpha$ measurably increased secretion of both IL-8 and IL-1 β while negatively impacting barrier function, as measured by TEER and small molecule permeability. When hyperglycemia and $TNF\alpha$ were combined, MUC2 increased and ALP activity decreased in a manner similar to TNF α alone, although a synergistic effect was observed at the highest concentration of glucose tested (60 mM). Moreover, very high glucose concentrations (60 mM) potentiated the secretion of IL-8, suggesting the potential for a synergistic effect on tissue inflammation in vivo. Automated high content imaging of the colonic epithelial cells demonstrated little impact of glucose on cell shape and size. In contrast, the cells were extraordinarily sensitive to $TNF\alpha$ with this inflammatory molecule acting as the dominant modulator of morphology relative to the effect of glucose. Based on the results of these studies, we conclude that hyperglycemia may potentiate inflammatory cytokine production, but has limited impact on intestinal permeability. In contrast, TNF α exposure has a profound effect on intestinal permeability in a dose-dependent manner.

The results of this study suggest that control of inflammation rather than glucose may be the dominant factor in maintaining intestinal homeostasis. However, hyperglycemiaenhanced inflammation (mediated by $TNF\alpha$) has important implications for critically ill individuals experiencing stress hyperglycemia in relation to their susceptibility to increased intestinal permeability and infection. Intriguingly, the observed increase in MUC2 presence during inflammation that was potentiated by high glucose (60 mM) does not have a precedent from primary colonic epithelial models, and conflicts with the status of $TNF\alpha$ as a known inducer of Notch signaling (i.e. favoring absorptive lineages) [71]. Based on our observations and the results of previous studies [24], we posit that the protective mucus barrier is differentially regulated by Notch and MAPK signaling during inflammation, warranting further mechanistic investigations into the context and relative contribution of each pathway. These future studies could be bolstered by the inclusion of wound healing assays [84, 85] and the enrichment of goblet cell lineages [86] for a richer understanding of how metabolism and inflammation contribute to intestinal injury-repair cycles [87]. Both of the above protocols are readily compatible with the hydrogel monolayer platform utilized in this report, with 3D culture systems presenting substantial obstacles against their implementation. In summary, we have demonstrated the utility of the gradient crosslinked hydrogel platform for investigating the impact of hyperglycemia and inflammation on primary colonic epithelial cells. This preliminary demonstration utilized intestinal stem cells derived from a human cadaveric donor,

and future conclusions will be strengthened by the inclusion of multiple human specimens derived from donors of varying genders, ages, and disease states [88]. We acknowledge that the current platform lacks additional features that would be of value in fully replicating intestinal physiology, most notably the microbiome and inflammatory cells. Recent progress is making such a combined system feasible, which will further efforts to elucidate the role of factors such as hyperglycemia and inflammatory cytokines on intestinal pathophysiology [86,

SUPPLEMENTARY DATA

Supplementary data are available at INTBIO Journal online.

ACKNOWLEDGEMENTS

The authors wish to thank Prof. Scott T. Magness for procurement of the intestinal tissue specimen.

FUNDING

This work was supported by the National Institute of Diabetes and Digestive and Kidney Diseases (NIDDK) at the National Institutes of Health (R01 DK109559).

CONFLICT OF INTEREST STATEMENT

N.L.A. and C.E.S. report a financial interest in Altis Biosystems, Inc. The remaining authors declare no competing financial inter-

REFERENCES

- 1. Bar-Or D, Rael LT, Madayag RM et al. Stress hyperglycemia in critically ill patients: insight into possible molecular pathways. Front Med (Lausanne) 2019;6:54.
- 2. Brealey D, Singer M. Hyperglycemia in critical illness: a review. J Diabetes Sci Technol 2009;3:1250-60.
- 3. Davis G, Fayfman M, Reyes-Umpierrez D et al. Stress hyperglycemia in general surgery: why should we care? J Diabetes Complications 2018;32:305-9.
- 4. Goyal N, Kaur R, Sud A et al. Non diabetic and stress induced hyperglycemia [SIH] in orthopaedic practice what do we know so far? J Clin Diagn Res 2014;8:LH01–3.
- 5. Mi D, Wang P, Yang B et al. Correlation of hyperglycemia with mortality after acute ischemic stroke. Ther Adv Neurol Disord 2018;11:1756285617731686.
- 6. Peacock TS. Perioperative hyperglycemia: a literature review. AORN J 2019;109:80-6.
- 7. Preechasuk L, Suwansaksri N, Ipichart N et al. Hyperglycemia and glycemic variability are associated with the severity of sepsis in nondiabetic subjects. J Crit Care 2017;38:319-23.
- 8. Wernly B, Lichtenauer M, Hoppe UC et al. Hyperglycemia in septic patients: an essential stress survival response in all, a robust marker for risk stratification in some, to be messed with in none. J Thorac Dis 2016;8:E621-4.
- 9. Sommerfield AJ, Deary IJ, Frier BM. Acute hyperglycemia alters mood state and impairs cognitive performance in people with type 2 diabetes. Diabetes Care 2004;27:2335-40.

- 10. Szumita PM, Gilmore JF. Admission hyperglycemia in sepsis is associated with poor outcomes: where do we go from here? J Thorac Dis 2016;8:E567-70.
- 11. Salinas PD, Mendez CE. Glucose management technologies for the critically ill. J Diabetes Sci Technol 2019;13:
- 12. Adelman MW, Woodworth MH, Langelier C et al. The gut microbiome's role in the development, maintenance, and outcomes of sepsis. Crit Care 2020;24:278.
- 13. Tamburini FB, Andermann TM, Tkachenko E et al. Precision identification of diverse bloodstream pathogens in the gut microbiome. Nat Med 2018;24:1809-14.
- 14. Dandoy CE, Kim S, Chen M et al. Incidence, risk factors, and outcomes of patients who develop mucosal barrier injurylaboratory confirmed bloodstream infections in the first 100 days after allogeneic hematopoietic stem cell transplant. JAMA Netw Open 2020;3:e1918668.
- 15. Posteraro P, De Maio F, Menchinelli G et al. First bloodstream infection caused by Prevotella copri in a heart failure elderly patient with Prevotella-dominated gut microbiota: a case report. Gut Pathog 2019;11:44.
- 16. Moron R, Galvez J, Colmenero M et al. The importance of the microbiome in critically ill patients: role of nutrition. Nutrients 2019;11:1-17.
- 17. Suzuki T. Regulation of intestinal epithelial permeability by tight junctions. Cell Mol Life Sci 2013;70:631-59.
- 18. Al-Sadi R, Bolvin M, Ma T. Mechanism of cytokine modulation of epithelial tight junction barrier. Front Biosci 2013;14:2765-78.
- 19. Andrews C, McLean MH, Durum SK. Cytokine tuning of intestinal epithelial function. Front Immunol 2018;9:1270.
- 20. Capaldo CT, Nusrat A. Cytokine regulation of tight junctions. Biochim Biophys Acta 2009;1788:864-71.
- 21. Onyiah JC, Colgan SP. Cytokine responses and epithelial function in the intestinal mucosa. Cell Mol Life Sci
- 22. Yajima S, Morisaki H, Serita R et al. Tumor necrosis factoralpha mediates hyperglycemia-augmented gut barrier dysfunction in endotoxemia. Crit Care Med 2009;37:1024-30.
- 23. Adegbola SO, Sahnan K, Warusavitarne J et al. Anti-TNF therapy in Crohn's disease. Int J Mol Sci 2018;19:1-21.
- 24. Leppkes M, Roulis M, Neurath MF et al. Pleiotropic functions of TNF-alpha in the regulation of the intestinal epithelial response to inflammation. Int Immunol 2014;26:509-15.
- 25. Ma TY, Iwamoto GK, Hoa NT et al. TNF-a-induced increase in intestinal epithelial tight junction permeability requires NF-kB activation. American journal of gastroenterology and liver. Phys Ther 2004;286:G367-G76.
- 26. Van Hauwermeiren F, Vandenbroucke RE, Grine L et al. TNFR1-induced lethal inflammation is mediated by goblet and Paneth cell dysfunction. Mucosal Immunol 2015;8: 828-40
- 27. Xiao YT, Yan WH, Cao Y et al. Neutralization of IL-6 and TNFalpha ameliorates intestinal permeability in DSS-induced colitis. Cytokine 2016;83:189-92.
- 28. Lopez-Posadas R, Neurath MF, Atreya I. Molecular pathways driving disease-specific alterations of intestinal epithelial cells. Cell Mol Life Sci 2017;74:803-26.
- 29. Brockmann L, Giannou AD, Gagliani N et al. Regulation of TH17 cells and associated cytokines in wound healing, tissue regeneration, and carcinogenesis. Int J Mol Sci 2017;
- 30. Garcia-Carbonell R, Yao SJ, Das S et al. Dysregulation of intestinal epithelial cell RIPK pathways promotes chronic

- Inflammation in the IBD gut. Front Immunol 2019;10:
- 31. Novotny-Smith CL, Zorbas MA, Irimura T et al. Downmodulation of epidermal growth factor accompanies TNFinduced differentiation of the DiFi human adenocarcinoma cell line toward a goblet-like phenotype. J Cell Physiol 1993;157:253-62.
- 32. Enss M, Cornberg M, Wagner S et al. Proinflammatory cytokines trigger MUC gene expression and mucin release in the intestinal cancer cell line LS180. Inflamm Res 2000;49:162-9.
- 33. Aleman L, Guerrero J. Sepsis hyperglycemia in the ICU: from the mechanism to the clinic. Rev Med Chil 2018;146:502–10.
- 34. Marik PE, Raghavan M. Stress-hyperglycemia, insulin and immunomodulation in sepsis. Intensive Care Med 2004;30:748-56.
- 35. Diebel LN, Liberati DM, Martin JV. Acute hyperglycemia increases sepsis related glycocalyx degradation and endothelial cellular injury: a microfluidic study. Am J Surg 2019;217:1076-82.
- 36. Esposito K, Nappo F, Marfella R et al. Inflammatory cytokine concentrations are acutely increased by hyperglycemia in humans: role of oxidative stress. Circulation 2002;106:2067-72.
- 37. Grosick R, Alvarado-Vazquez PA, Messersmith AR et al. High glucose induces a priming effect in macrophages and exacerbates the production of pro-inflammatory cytokines after a challenge. J Pain Res 2018;11:1769-78.
- 38. Yu W, Li W, Li J. Influence of acute hyperglycemia in human sepsis on inflammatory cytokine and counterregulatory hormone concentrations. World J Gastroenterol 2003;9:1824-7.
- 39. Giri B, Dey S, Das T et al. Chronic hyperglycemia mediated physiological alteration and metabolic distortion leads to organ dysfunction, infection, cancer progression and other pathophysiological consequences: an update on glucose toxicity. Biomed Pharmacother 2018;107:306-28.
- 40. Niu S, Bian Z, Tremblay A et al. Broad infiltration of macrophages leads to a proinflammatory state in streptozotocin-induced hyperglycemic mice. J Immunol 2016;197:3293-301.
- 41. Vermette D, Hu P, Canarie MF et al. Tight junction structure, function, and assessment in the critically ill: a systematic review. Intensive Care Med Exp 2018;**6**:37.
- 42. Tiruvoipati R, Chiezey B, Lewis D et al. Stress hyperglycemia may not be harmful in critically ill patients with sepsis. J Crit Care 2012;27:153-8.
- 43. Allam O, Samarani S, Mehraj V et al. HIV induces production of IL-18 from intestinal epithelial cells that increases intestinal permeability and microbial translocation. PLoS One 2018;**13**:e0194185.
- 44. Cui W, Li LX, Sun CM et al. Tumor necrosis factor alpha increases epithelial barrier permeability by disrupting tight junctions in Caco-2 cells. Braz J Med Biol Res 2010;43:330–7.
- 45. Dutton JS, Hinman SS, Kim R et al. Primary cell-derived intestinal models: recapitulating physiology. Trends Biotechnol 2019;37:744-60.
- 46. Luo PL, Wang YJ, Yang YY et al. Hypoxia-induced hyperpermeability of rat glomerular endothelial cells involves HIF-2alpha mediated changes in the expression of occludin and ZO-1. Braz J Med Biol Res 2018;**51**:e6201.
- 47. Pearce SC, Al-Jawadi A, Kishida K et al. Marked differences in tight junction composition and macromolecular permeability among different intestinal cell types. BMC Biol 2018; **16**:19.

- 48. Qu W, Yuan X, Zhao J et al. Dietary advanced glycation end products modify gut microbial composition and partially increase colon permeability in rats. Mol Nutr Food Res 2017;
- 49. Suzuki T, Yoshinaga N, Tanabe S. Interleukin-6 (IL-6) regulates claudin-2 expression and tight junction permeability in intestinal epithelium. J Biol Chem 2011;286:31263-71.
- 50. Gunasekara DB, Speer J, Wang Y et al. A monolayer of primary colonic epithelium generated on a scaffold with a gradient of stiffness for drug transport studies. Anal Chem 2018;90:13331-40.
- 51. Hinman SS, Wang Y, Kim R et al. In vitro generation of selfrenewing human intestinal epithelia over planar and shaped collagen hydrogels. Nat Protoc 2021;16:352-82.
- 52. Wang Y, DiSalvo M, Gunasekara DB et al. Self-renewing monolayer of primary colonic or rectal epithelial cells. Cell Mol Gastroenterol Hepatol 2017;4:165-82.
- 53. Wang Y, Gunasekara DB, Reed MI et al. A microengineered collagen scaffold for generating a polarized crypt-villus architecture of human small intestinal epithelium. Biomaterials 2017;128:44-55.
- 54. Sato T, Stange DE, Ferrante M et al. Long-term expansion of epithelial organoids from human colon, adenoma, adenocarcinoma, and Barrett's epithelium. Gastroenterology 2011;141:1762-72.
- 55. Miyoshi H, Stappenbeck TS. In vitro expansion and genetic modification of gastrointestinal stem cells in spheroid culture. Nat Protoc 2013;8:2471-82.
- 56. Bhatt AP, Gunasekara DB, Speer J et al. Nonsteroidal antiinflammatory drug -induced leaky gut modeled using polarized monolayers of primary human intestinal epithelial cells. ACS Infect Dis 2018;4:46-52.
- 57. Hinman SS, Huling J, Wang Y. et al Magnetically-propelled fecal surrogates for modeling the impact of solidinduced shear forces on primary colonic epithelial cells. bioRxiv. 2021:Pre-Print. February 18, 2021, doi 10.1101/2021.02.18.431336, preprint: not peer reviewed.
- 58. Lim JS. Two-Dimensional Signal and Image Processing. Prentice Hall, Englewood Cliffs, NJ, 1990.
- 59. Otsu N. A threshold selection method from gray-level histograms. IEEE Trans Syst Man Cybern 1979;9:62-6.
- 60. Lee T, Kashyap R. Building skeleton models via 3-D medial surface/axis thinning algorithms. CVGIP. Graph Models Image Process 1994;56:462-78.
- 61. Vincent L. Morphological grayscale reconstruction in image analysis: applications and efficient algorithms. IEEE Trans Image Process 1993;**2**:176–201.
- 62. Meyer F. Topographic distance and watershed lines. Signal Process 1993;38:113-25.
- 63. Speer JE, Gunasekara DB, Wang Y et al. Molecular transport through primary human small intestinal monolayers by culture on a collagen scaffold with a gradient of chemical cross-linking. J Biol Eng 2019;13:36.
- 64. Speer JE, Wang Y, Fallon JK et al. Evaluation of human primary intestinal monolayers for drug metabolizing capabilities. J Biol Eng 2019;13:82.
- 65. Giacomelli C, Natali L, Nisi M et al. Negative effects of a high tumour necrosis factor- α concentration on human gingival mesenchymal stem cell trophism: the use of natural compounds as modulatory agents. Stem Cell Res Ther 2018;9:
- 66. Grell M, Wajant H, Zimmermann G et al. The type 1 receptor (CD120a) is the high-affinity receptor for soluble tumor necrosis factor. Cell Biol 1998;95:570-5.

- 67. Wu Y, Bressette D, Carrell JA et al. Tumor necrosis factor (TNF) receptor superfamily member TACI is a high affinity receptor for TNF family members APRIL and BLyS. J Biol Chem 2000;**275**:35478–85.
- 68. Zhao S, Jiang J, Jing Y et al. The concentration of tumor necrosis factor-α determines its protective or damaging effect on liver injury by regulating yap activity. Cell Death Dis
- 69. VanDussen KL, Carulli AJ, Keeley TM et al. Notch signaling modulates proliferation and differentiation of intestinal crypt base columnar stem cells. Development 2012;139:
- 70. Kaiko GE, Ryu SH, Koues OI et al. The colonic crypt protects stem cells from microbiota-derived metabolites. Cell 2016;165:1708-20.
- 71. Fazio C, Inflammation RL. Notch signaling: a crosstalk with opposite effects on tumorigenesis. Cell Death Dis
- 72. Ruder B, Atreya R, Becker C. Tumour necrosis factor alpha in intestinal homeostasis and gut related diseases. Int J Mol Sci 2019;20:1-21.
- 73. Hu R, Xia CQ, Butfiloski E et al. Effect of high glucose on cytokine production by human peripheral blood immune cells and type I interferon signaling in monocytes: implications for the role of hyperglycemia in the diabetes inflammatory process and host defense against infection. Clin Immunol 2018;195:
- 74. Fischer A, Gluth M, Pape UF et al. Adalimumab prevents barrier dysfunction and antagonizes distinct effects of TNFalpha on tight junction proteins and signaling pathways in intestinal epithelial cells. Am J Physiol Gastrointest Liver Physiol 2013;**304**:G970–9.
- 75. Shin W, Kim HJ. Intestinal barrier dysfunction orchestrates the onset of inflammatory host-microbiome cross-talk in a human gut inflammation-on-a-chip. Proc Natl Acad Sci U S A 2018;**115**:E10539–E47.
- 76. Thaiss CA, Levy M, Grosheva I et al. Hyperglycemia drives intestinal barrier dysfunction and risk for enteric infection. Science 2018;**359**:1376–83.
- 77. Gonzales GB, Van Camp J, Vissenaekens H et al. Review on the use of cell cultures to study metabolism, transport, and accumulation of flavonoids: from mono-cultures to co-culture systems. Compreh Rev Food Sci Food Saf 2015;**14**:741–54.
- 78. Sun H, Chow EC, Liu S et al. The Caco-2 cell monolayer: usefulness and limitations. Expert Opin Drug Metab Toxicol 2008;4:395-411.
- 79. Hidalgo IJ, Raub TJ, Borchardt RT. Characterization of the human colon carcinoma cell line (Caco-2) as a model system for intestinal epithelial permeability. Gastroenterology 1989:**96**:736-49.
- 80. Yamaura Y, Chapron BD, Wang Z et al. Functional comparison of human colonic carcinoma cell lines and primary small intestinal epithelial cells for investigations of intestinal drug permeability and first-pass metabolism. Drug Metab Dispos 2016;44:
- 81. Wnorowski A, Yang H, Progress WJC. Obstacles, and limitations in the use of stem cells in organ-on-a-chip models. Adv Drug Deliv Rev 2019;**140**:3–11.
- 82. Hinman SS, Kim R, Wang Y et al. Microphysiological system design: simplicity is elegance. Curr Opin Biomed Eng 2020;13:94-102.

- 83. Naumovska E, Aalderink G, Wong Valencia C et al. Direct on-chip differentiation of intestinal tubules from induced pluripotent stem cells. Int J Mol Sci 2020;
- 84. Liang CC, Park AY, Guan JL. In vitro scratch assay: a convenient and inexpensive method for analysis of cell migration in vitro. Nat Protoc 2007;2:329-33.
- 85. Rodriguez LG, Wu X, Guan JL. Wound-healing assay. Methods Mol Biol 2005;294:23-9.
- 86. Wang Y, Kim R, Sims CE et al. Building a thick mucus hydrogel layer to improve the physiological relevance of in vitro primary colonic epithelial models. Cell Mol Gastroenterol Hepatol 2019;8:653-5 e5.
- 87. Wang Y, Chiang IL, Ohara TE et al. Long-term culture captures injury-repair cycles of colonic stem cells. Cell 2019;**179**:1144–59 e15.
- 88. Sachs N, de Ligt J, Kopper O et al. A living biobank of breast cancer organoids captures disease heterogeneity. Cell 2018;172:373-86 e10.
- 89. Kim R, Attayek PJ, Wang Y et al. An in vitro intestinal platform with a self-sustaining oxygen gradient to study the human gut/microbiome interface. Biofabrication 2019;**12**:015006.
- 90. Wang Y, Kim R, Hwang SJ et al. Analysis of interleukin 8 secretion by a stem-cell-derived human-intestinalepithelial-monolayer platform. Anal Chem 2018;90:11523-30.